On the intra-subject similarity of hand vein patterns in biometric recognition

Rıdvan Salih Kuzu, Emanuele Maiorana, Patrizio Campisi

{rıdvansalih.kuzu, emanuele.maiorana, patrizio.campisi} @uniroma3.it [1]

Roma Tre University, Via Vito Volterra 62, Rome, Italy, 00146

Corresponding Author:

Emanuele Maiorana

Email: emanuele.maiorana@uniroma3.it

[1]Please cite this work as: Ridvan Salih Kuzu, Emanuele Maiorana, Patrizio Campisi, On the intra-subject similarity of hand vein patterns in biometric recognition, Elsevier Expert Systems with Applications, in press, 2021

Rıdvan Salih Kuzu[a], Emanuele Maiorana[a,*], Patrizio Campisi[a]

[a]*Roma Tre University, Via Vito Volterra 62, Rome, Italy, 00146*

Abstract

In these years, biometric recognition based on hand vein patterns is receiving an always increasing attention from both industry and academia, thanks to the advantages it offers with respect to conventional approaches, such as those relying on fingerprint, iris, or face. Nevertheless, there are still several properties of vein traits that need to be investigated and well understood. In this paper, we here analyze the level of similarity, evaluated in terms of recognition rate of a biometric system, of vein patterns in the fingers, palms, and dorsa of a person's left and right hands. In other words, we analyse whether a subject, enrolled using vein patterns, either finger-vein, palm-vein, dorsal-vein, from one hand, can be recognized using the homologous patterns from the other hand. Our investigation is conducted using deep-learning-based feature extraction approaches, three different vein modalities, and four different databases. The obtained experimental results show that corresponding fingers, palms, and dorsal regions from different hands of the same subject show more resemblance with respect to the traits from the same hand of different persons. Furthermore, our findings point out that similarities among vein patterns in corresponding fingers could be used for recognition purposes, while this still cannot be applied to palm and dorsum vein patterns.

Keywords: Biometric Recognition, Vein Patterns, Deep Learning

*Corresponding author.

1. Introduction

The demand for applying biometric recognition technologies in real-life applications, ranging from consumer devices to border control, from surveillance to access control and financial services, to give few examples, is growing at an increasing pace. Face, fingerprint, iris, and voice are the most mature biometric traits currently exploited to automatically recognize people. Among the emerging modalities, both industry and academia are showing an always growing interest towards the exploitation of hand vein patterns, due to the several advantages such characteristics guarantee with respect to more established biometric modalities. In fact, vein patterns such as those present in the fingers, the palms, and the dorsa of our hands are more robust to presentation attacks than other biometric identifiers, being not publicly exposed. In addition, their acquisition can be made using a contactless approach, thus increasing user convenience.

Even though several systems, employed in real-life applications, already employ hand vein patterns for automatic biometric recognition, there are still several properties of these traits which have to be properly analyzed. Specifically, in this paper, within a biometric recognition framework, we investigate the existence of similar characteristics in the vein patterns of the right and left hands of the same subject. In more detail, the present study stems from our previous analysis (Piciucco et al., 2019), and provides the following additional insights:

- in this contribution, we perform a deeper analysis with respect to the one carried out in (Piciucco et al., 2019), where we have preliminary evaluated the existence of similar characteristics in the vein patterns of the corresponding fingers, belonging to the right and left hands of an individual. More specifically, in this paper we check the level of similarity among vein patterns of the right and left hand palms, of the right and left hand dorsa, and of the corresponding fingers in the right and the left hands;
- four distinct databases, to evaluate the existence of similar patterns in the veins of left and right hands, are here exploited, thus providing a more

statistical significant analysis of the one in (Piciucco et al., 2019), where a single dataset has been considered;

- hand-crafted characteristics have been mostly considered in (Piciucco et al., 2019) to speculate about the similarity of left and right finger-vein patterns. On the other hand, we here resort to deep learning approaches to automatically process the considered traits. Specifically, we use a recently-introduced loss function (Deng et al., 2019) to improve the discriminability of the extracted features, even when performing an open-set training procedure. Furthermore, two distinct learning strategies are employed to derive the discriminative characteristics upon which our analyses are carried out. One of them has been specifically designed to look for similarities between the vein patterns of the right and left hands of a subject. As it will be shown in the following, the employed approach is able to locate similar characteristics between corresponding pairs of vein patterns, differently from the approaches presented in (Piciucco et al., 2019).

It is worth remarking that, to the best of our knowledge, no anatomical study has specifically investigated the existence of similarities between vein patterns in the left and right hands of a person. The present study, within the biometric framework, sheds a light on the topic using deep learning strategies, specifically designed to find such similarities.

The paper is structured as follows: in Section 2 we report a review of the state of the art about the evaluation of possible similarities between left and right instances of different biometric traits. Section 3 deals specifically with hand vein patterns, presenting the physiological background of the acquisition process, and the state-of-the-art papers. The frameworks employed in our analysis to process the considered hand vein patterns are detailed in Section 4, while the performed experimental tests, together with a discussion about the obtained results, are outlined in Section 5. Eventually, some conclusions are drawn in Section 6.

2. Similarities in Left and Right Biometric Traits of a Person

Potential similarities between biometric traits belonging to the right and left sides of the human body have been already investigated in the past within the biometric scenarios. The potential interchangeability of the enrolled biometric traits could lead to some benefits in real-world systems, such as avoiding re-enrollment in case one trait becomes no more usable, temporarily or permanently, thus increasing user convenience and flexibility.

Moreover, a clear understanding about the existence of such similarities could be beneficial to optimize the design of experimental protocols, deciding whether to exclude, from the samples used to estimate the distributions of the impostors' recognition scores, the traits belonging to a body side other than the one considered for the enrolment of a genuine subject. As a matter of fact, as a precaution, recommendations in the ISO/IEC 19795 standard (Information technology – Biometric performance testing and reporting) suggest to avoid the usage, as impostor attempts, of comparisons between left and right instances of the same biometric trait of a subject, since intra-individual differences are likely lower than inter-individual ones (International Organization for Standardization, 2006, paragraph 7.6.1.3).

The first exploration regarding possible similarities between left and right biometric traits of a subject has been reported in (Bowyer et al., 2010), where the left iris of each user is compared against the right ones of all considered subjects, relying on the binary iris template representation proposed by (Daugman, 2004). The obtained distance distributions, referred to comparisons between data from the same subjects and from different subjects, are basically overlapped, confirming that the left and right irises of the same person do not match any more closely than do the irises of different persons. Nonetheless, tests relying on human observers, which have been asked to judge whether a pair of left and right eye images have been taken from the same person, have been also reported in (Bowyer et al., 2010). Interestingly, the involved observers, without any specific knowledge on iris anatomy, correctly classified over 86% of the pre-

sented image pairs, a percentage slightly lowered to 83% in case either only the iris region, or only the periocular region, have been shown. Such results support the hypothesis that similar patterns between left and right irises actually exist, yet the employed automated iris biometric technology is not able to recognize them as effectively as humans can, suggesting that people interpret iris texture in a quite different way than iris biometric systems. As a side note, analogous results have been also reported in (Hollingsworth et al., 2011), where it has been shown that humans are also able to correctly match the irises of identical twins, while these latter are as different as those of unrelated people for a standard iris biometric recognition algorithm.

An investigation about the similarity of left and right ears of the same subjects has been conducted in (Claes et al., 2015). Tests relying on features extracted from 3D samples, and performed by comparing left ears against right ones, with instances from the same subject generating genuine scores and samples from different subjects resulting in impostor attempts, have shown that it is possible to achieve an equal error rate (EER) of 11%. This result, obtained by manually selecting specific substructures of the ear out of the available feature space, shows that differences among individuals are larger that those between left and right instances of the same subject.

A biometric recognition framework has been also exploited in (Xu et al., 2015) to infer about the similarity of left and right palmprints. Also in this case, each left palmprint, in the considered database, has been compared against every right palmprint of each subject, with the computed scores considered as genuine if originated from samples of the same person, and impostor otherwise. EERs at 24.22% and 35.82% have been obtained on two distinct dataset, showing that also the left and right palmprints of the same person generally have higher similarity than those from different subjects. In (Kumar et al., 2016), experiments similar to the ones in (Xu et al., 2015) have been carried out, yet exploiting deep learning strategies, in addition to state-of-the-art methods relying on hand-crafted features, to derive the palmprint representations employed in the performed tests. Training a network by assigning the same label to left

and right palmprints of the same user, an EER equal to 9.25% has been obtained comparing samples of different hands of the same individual, and samples from different persons. The achieved result has shown the superiority of deep learning strategies, over hand-crafted approaches, in finding similarities between left and right biometric instances of the same subject. It has yet to be remarked that a closed-set testing procedure, where tests are carried out over the same subjects employed for network training, has been adopted in (Kumar et al., 2016) to evaluate the effectiveness of the employed convolutional neural network (CNN) as feature extractor, therefore affecting the reliability and generalizability of the obtained results.

Tests on retinas have been recently conducted in (Biswas et al., 2019). A CNN trained only for dimensionality reduction has been there employed as feature extraction, and the scores generated by comparing templates associated to the two retinas of the same person have been compared against those obtained when comparing samples from different users. The observed behavior testifies that also the left and right retinas of a person have more similarity than the retinas from two distinct persons. As in (Bowyer et al., 2010), subjective tests relying on the judgement of human volunteers about the similarity of two retinas have been also performed. Also in this case, humans seem to possess an higher capability than currently available algorithms to detect similarities between left and right traits of the same person.

As mentioned in Section 1, the similarity of left and right finger-vein patterns has been preliminarily investigated in our previous work (Piciucco et al., 2019), where we have observed that, although corresponding fingers from different hands of the same subject show more resemblance than those from different persons, the similarities found through hand-crafted features are not significant enough to be exploited in a biometric recognition systems. In fact, EERs higher than 30% have been estimated in (Piciucco et al., 2019) using left and right finger-vein patterns as genuine comparisons.

Therefore, the literature suggests that hand-crafted features, despite allowing to perform standard biometric recognition, may not be suited for capturing

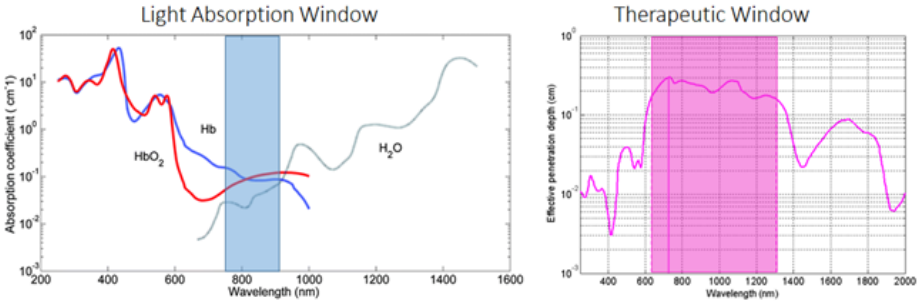

Figure 1: Light absorption (left) and therapeutic (right) windows

the similarities between left and right traits of the same individual, even if these similarities actually exist and are evident to a human observer. Conversely, leveraging on deep learning strategies could instead be beneficial to emulate human learning and discriminating capabilities, specifically looking for the desired similarities, as already shown for palmprints in (Kumar et al., 2016).

Within this framework, in this paper, we expand our previous research (Piciucco et al., 2019) not only by considering palm- and dorsal-vein patterns, in addition to finger-veins, but also employing a CNN-based approach to look for similarities between the vein patterns of the right and left hands of a subject, instead of resorting to hand-crafted features, in order to better mimic the human evaluation capability. The following sections give more details regarding the considered biometric traits and the exploited processing strategies.

3. Hand Vein Biometric Recognition

In the late 80s, vascular patterns have been introduced as a potential biometric identifier (Rice, 1987), exploiting the properties of near-infrared (NIR) light to pass through human skin, and to be absorbed by blood haemoglobin in vein vessels. These characteristics are described by the *light absorption window* and the *therapeutic window* depicted in Figure 1:

- *light absorption window*: the wavelengths interval [700, 900] *nm* where the oxygenated and the deoxygeneted haemoglobin reaches its light absorption

peak between (DeoxyHb: 760nm; OxyHb: 900nm);

- *therapeutic window*: the wavelengths interval, [650, 1350] nm, where the light has its maximum depth of penetration in the human tissue.

As a consequence, the NIR light absorption capability of haemoglobin makes the blood vessels appearing darker while the remaining parts of the body reflect the light in specific NIR wavelength windows. Thus, vascular patterns can be acquired using a NIR camera, equipped with a NIR illuminator working either in the transmission or the reflection modality.

A brief overview about the state of the art on biometric recognition systems exploiting finger, hand, and dorsal vein patterns, is reported in the following, and a summary of the main features of the systems operating in the verification modality is given in Table 1. A deeper evaluation of the state of the art on vein biometric recognition has been recently provided in (Uhl et al., 2020).

3.1. Traditional Approaches

The methods employed to process vein patterns in biometric recognition systems are typically distinguished into profile-based and feature-based approaches. The former category is focused on the extraction of the cross-sectional contour of the veins in an image. For instance, the maximum curvature approach (Miura et al., 2007) leads to robust performance on different finger-vein databases. Instead, feature-based approaches rely on the assumption that the vein regions areas are darker compared to remaining parts of the hand, and line-like shapes are interpreted as vein patterns in the contour of vein images. For example, methods extracting minutiae features on the line patterns, and using the Hausdorff distance in spatial domain, e.g. (Wang et al., 2008), to measure their similarities, belong to the latter category.

In more detail, early attempts to use palm vein biometrics relied on feature-based approaches on a dataset, namely the PolyU-P palm vein database, composed by RGB images in both the visible and NIR sub-bands (Zhang et al., 2009). Both palm print features from the RGB sub-bands, and palm vein features from the NIR sub-band, have been extracted using texture-based coding

Reference	Vein Pattern	Database			Proposed System		EER
		Name	# Users	Comment	Feature Extraction	Matching	(in %)
(Wang et al., 2020)	Dorsal Finger Palm Palm	OWN FV-USM PUT PolyU-P	200 123 50 200	Data from distinct sessions are separately used for training and testing, yet the same subjects are considered in the two phases (closed-set scenario).	Multi-weighted Co-occurence Descriptor Encoding	Large Margin Distribution Machine	0.015 0.307 0.615 0.017
(Kuzu et al., 2020a)	Finger Finger Palm Palm Dorsal	SDUMLA PolyU-F PolyU-P CASIA Bosphorus	636 312 500 200 100	Data from distinct sessions are separately used for training and testing, with different subjects considered in the two phases (open-set scenario).	Modified Densenet-161 with AAMP	Channel-wise Euclidian Distance	0.02 1.87 0.00 1.12 2.58
(Ahmad et al., 2019)	Palm	PolyU-P PUT VERA OWN	250 50 110 50	Template generation performed using 4 samples from each genuine subject, exploiting cancelable transformation to ensure preserving the privacy.	ROI Enhancement Followed by Wave Atom Transform	Normalized Hamming Distance	1.98 0.00 3.05 1.49
(Wu et al., 2019)	Palm	CASIA OWN	100 250	It is not specified whether data taken during the same session are used for training and testing.	Haar-Wavelet Decomposition and Partial Least Square	Euclidian Distance	0.029 0.405
(Qin et al., 2019)	Palm	PolyU-P CASIA	250 100	Data from distinct sessions are separately used for training and testing, yet the same subjects are considered in the two phases (closed-set scenario).	Iterative Deep Belief Network	Hamming Distance	0.01 0.33
(Yang et al., 2019)	Finger	THU-FVFDT2 SDUMLA	610 106	THU-FVFDT2 splitted into disjoint sets for training, validation, and test. SDUMLA used for verification.	Generative Adverserial Networks for Finger Vein (FV-GAN)	Cross Correlation on Binarized Templates	1.12 0.94
(Thapar et al., 2019)	Palm	PolyU-P CASIA IITI	250 100 185	Data divided in two sets having the same size, the first half for training and the other for testing.	U-Net like Decoder-Encoder CNN Architecture	Siamese Matching Network	0.66 3.71 0.93
(Song et al., 2019)	Finger	SDUMLA PolyU-F	106 156	Data divided in two sets having the same size. Tests on PolyU-F conducted using same-session data for training and testing.	Densenet-161 on Composite Finger Images	Shift Matching and Minimum Rule	2.35 0.33
(Zhong et al., 2019)	Palm Dorsal Multi	PolyU-P NGX Private	250 420 57	Three dorsal vein dataset is combined and named as NGX (NCUT + GPDS + XJTU). Multi-vein dataset is composed of palm and dorsal vein	Deep Hashing Network Biometric Graph Matching	SVM Hamming Distance	0.01 3.91 0.00
(Pan et al., 2019)	Palm Palm Palm Dorsal	PolyU-P PUT Private Private	250 50 224 224	The private database is acquired as 2 sessions, each includes 5 images.	VGG-16 combined with LMP-PSP and PCA	SVM	0.04 0.58 1.74 1.28
(Wang et al., 2018)	Palm Dorsal	PolyU-P OWN	250 200	It is not specified whether data taken during the same session are used for training and testing.	Spatial Pyramid Pooling on pre-trained VGG16	SVM Classifier	0.07 0.06
(Fang et al., 2018)	Finger	MMCBNU SDUMLA	100 106	Data from the same subjects are considered for testing and training (closed-set scenario).	2-Channel Network, 2-Stream Network, and Selective Network	SVM Classifier with Linear Kernel	0.10 0.47
(Yang et al., 2018)	Finger	SDUMLA PolyU-F	106 105	Tests conducted in same- and different-session conditions for training and testing (results from the latter scenario here reported).	Anatomy Structure Analysis based Vein Extraction (ASAVE)	Elastic Matching	1.39 2.91
(Jalilian & Uhl, 2018)	Finger	SDUMLA UTFVP	106 60	Tests conducted dividing each dataset into two disjoint subsets. Cross-database conditions also considered.	U-Net, RefineNet, SegNet	Cross Correlation on Binarized Templates	2.63 0.64
(Xie & Kumar, 2017)	Finger	PolyU-F	156	Training and testing conducted on distinct users.	Modified VGG-16 with Supervised Discrete Hashing	Hamming Distance	9.77
(Kauba et al., 2016)	Finger	UTFVP	60	Parameter tuning performed using 10% of available data, the rest employed to estimate EER.	Feature Level Fusion	Cross Correlation on Binarized Templates	0.19
(Das et al., 2014)	Wrist	PUT	50	Data from the same sessions and the same subjects used for training and testing (closed-set scenario).	Discrete Meyer Wavelet and Local Binary Patterns	SVM Classifier	0.79
(Kabaciński & Kowalski, 2011)	Wrist	PUT	50	Training and testing on data from different sessions.	Discrete Fourer Transform and Gradient-based Segmentation	Cross Correlation on Binarized Templates	2.19
(Yuksel et al., 2011)	Dorsal	Bosphorus	100	Different environmental scenarios considered in tests.	Fusion of LEM, NMF and ICA	Hausdorff Distance, Cosine Distance	2.25
(Kumar & Zhou, 2011)	Finger	PolyU-F	156	Tests conducted in same- and different-session conditions for training and testing.	Radon Transform and Gabor Filters	XOR-based Similarity Score	A: 2.45 B: 0.08
(Zhou & Kumar, 2011)	Palm	PolyU-P CASIA	250 100	Training and testing on data from different sessions.	Neighborhood Matching Radon Transform	Hamming Distance	0.21 1.37
(Zhang et al., 2009)	Palm	PolyU-P	250	Training and testing on data from same sessions.	Texture based Coding and Gabor Filters	Hamming Distance	0.01

Table 1: Vein based recognition systems: State-of-the-art

algorithm, and six Gabor filters along with different directions. An Equal Error Rate (EER) at 0.012% has been obtained after fusing the scores obtained from each channel.

In (Zhou & Kumar, 2011) the templates have been generated using a neighbourhood Radon transform, and a modified Hamming distance has been used for comparison. Tests performed on the PolyU-P dataset have resulted in EERs at 0.004%and 0.21% when respectively using either six or one enrollment samples per user. EERs at 1.37% and 0.51% have been obtained when using either one or three enrollment samples per user, respectively on images from the CASIA dataset (Hao et al., 2008). Experiments conducted on the PolyU-F finger vein dataset (Zhang et al., 2009) have provided an EER equal to 0.08% by fusing index and middle finger features (Kumar & Zhou, 2011). It is also there remarked

that a bias in the estimated performance can be introduced when comparing vein samples taken during the same session, with the consequent need, whenever possible, to compare vein samples captured in different occasions.

Tests on the SDUMLA (Yin et al., 2011) and PolyU-F have produced EERs at 1.39% and 0.38%, respectively, by using anatomy-structure analysis-based vein extraction (ASAVE) and elastic matching (Yang et al., 2018). On the UTFVP finger-vein database, an EER at 0.19% has been also obtained resorting to feature level fusion (Ton & Veldhuis, 2013).

Dorsal hand veins have been analyzed using a score level fusion approach relying on features extracted by line-edge map, non-negative matrix factorization, and independent component analysis (Yuksel et al., 2011). The reported EERs, on the Bosphorus dataset, for the naive tests implementing one-sample enrollment, and for tests implementing the enrollment stage with eight samples, are 8.18% and 2.25% respectively. It is worth remarking that, in the aforementioned studies, real-life conditions have been implemented in order to infer about the potential performance degradation.

3.2. Deep Learning-based Approaches

Recent progresses in deep learning are positively affecting the biometric field, among the others. The approach in (Radzi et al., 2016) is one the pioneering methods performing finger-vein recognition resorting to Convolutional Neural Networks (CNNs). Specifically, the employed architecture is a 4-layer CNN followed by a subsampling layer, while tests have been conducted on data recorded from 50 subjects. After this initial effort, there has been a flourishing of contributions applying deep learning to vein-based recognition systems.

Lightweight CNNs have also been exploited to extract templates from finger-vein samples taken from the MMCBNU (Lu et al., 2013) and the SDUMLA datasets (Fang et al., 2018). A selective network able to automatically choose one of them, depending on the features intra-class variations, has been built, with a support vector machine (SVM) having linear kernel employed for matching. Although promising results have been there reported, with EERs at 0.10%

on MMCBNU and 0.47% on SDUMLA, these results are biased, being obtained considering the same subjects during both training and testing, besides achieving these rates computing scores as averages over 5 comparisons.

Tests on PolyU and SDUMLA finger-vein datasets have been conducted also using the Densenet-161 architecture (Song et al., 2019). The authors have initially built composite samples from vein images by shifting each of them into various directions, and extracted features by using Densenet-161 thereafter. Experiments have been performed dividing the available data into two disjoint sets, with EERs obtained using a 2-fold cross-validation equal to 0.33% and 2.35% on PolyU-F and SDUMLA datasets, respectively. It has yet to be remarked that tests have been done considering only the first session of PolyU-F, therefore providing results which should be considered biased.

Different deep image segmentation algorithms, relying on U-Net, RefineNet, and SegNet frameworks, have been investigated in (Jalilian & Uhl, 2018), using human-annotated pixel-labels as ground-truth to create binary templates. EERs at 2.63% and 0.64% have been respectively reported on the SDUMLA and UTFVP finger-vein datasets. Features co-occurrence among different convolutional filters has been considered in (Wang et al., 2020). To test the robustness of their method, the authors have considered different vein modalities, namely dorsal-, palm-, and finger-vein. An innovative approach to perform on-the-fly finger vein acquisition, along with a novel deep learning architecture using both long short-term memory networks and convolutional neural networks, has been recently proposed (Kuzu et al., 2020b).

Also generative adversarial networks (GANs) have been used to analyze finger-vein patterns (Yang et al., 2019). Although GANs originally represent generative models for data synthesis, they have been employed to generate discriminative templates from vein patterns (Yang et al., 2019). The THU-FVFDT2 (Yang et al., 2009) and SDUMLA datasets, containing multiple sessions of finger-vein data from 610 and 106 unique subjects respectively, have been used for testing purposes. Specifically, the former dataset has been divided into distinct subsets for training, validation, and testing purposes, while

the latter has been used only to re-validate the proposed system. Recognition rates with EERs at 1.12% and 0.94% have been respectively reached on the two datasets.

4. Employed CNN-based Recognition System

In this Section, the network topology employed for our analysis is described, along with the network initialization and optimization.

4.1. Network Topology

In this study we exploit a modified Densenet-161 architecture (Huang et al., 2017), where the last layer is replaced with a Custom Embedder, as detailed in Table 2. To elaborate on the architecture, $224 \times 224 \times N_c$ input images are fed into the model, being N_c the number of available channels. The first convolution layer comprises 96 convolutional filters having size 7×7 and stride 2. A 3×3 maximum pooling with stride 2 is then used. Dense blocks and transition layers follow each other one by one prior to the Custom Embedder. Here, a dense block is composed of a sub-block of batch normalization (BN) - ReLU - 1×1 convolution, which is called as bottleneck layer, and a sub-block of BN - ReLU - 3×3 convolution with zero paddings on each side of input by one pixel. On the other hand, a transition layer connects two consecutive dense blocks by BN - ReLU - 1×1 Convolution and 2×2 average pooling having stride 2. The output of last dense block is fed into the Feature Embedder which is composed of following units: *i)* batch-normalization of input (vein) features followed by a 50% dropout regularisation employed to reduce overfitting, *ii)* one fully-connected (FC) layer comprising batch-normalization, consisting of $d = 1024$ neurons, being d the feature embedding size. The last FC layer of the network in Table 2 produces as output a vector with size U, depending on the total number of unique identities available in the considered training dataset.

In order to generate discriminative templates, following the latest achievements in CNN-based biometric recognition, the Additive Angular Margin Penalty

Layers		Input	Output
Convolution	7×7 conv (str.2)	$224 \times 224 \times 1$	$112 \times 112 \times 96$
Pooling	3×3 max pool (str.2)	$112 \times 112 \times 96$	$56 \times 56 \times 96$
Dense Block 1	$\begin{bmatrix} 1 \times 1 \text{ conv} \\ 3 \times 3 \text{ conv} \end{bmatrix} \times 6$	$56 \times 56 \times 96$	$56 \times 56 \times 384$
Transition 1	1×1 conv 2×2 avg pool (str.2)	$56 \times 56 \times 384$	$28 \times 28 \times 192$
Dense Block 2	$\begin{bmatrix} 1 \times 1 \text{ conv} \\ 3 \times 3 \text{ conv} \end{bmatrix} \times 12$	$28 \times 28 \times 192$	$28 \times 28 \times 768$
Transition 2	1×1 conv 2×2 avg pool (str.2)	$28 \times 28 \times 768$	$14 \times 14 \times 384$
Dense Block 3	$\begin{bmatrix} 1 \times 1 \text{ conv} \\ 3 \times 3 \text{ conv} \end{bmatrix} \times 36$	$14 \times 14 \times 384$	$14 \times 14 \times 2112$
Transition 3	1×1 conv 2×2 avg pool (str.2)	$14 \times 14 \times 2112$	$7 \times 7 \times 1056$
Dense Block 4	$\begin{bmatrix} 1 \times 1 \text{ conv} \\ 3 \times 3 \text{ conv} \end{bmatrix} \times 24$	$7 \times 7 \times 1056$	$7 \times 7 \times 2208$
Custom Embedder	7×7 avg pool BN 50% dropout	$7 \times 7 \times 2208$	1×2208
	FC layer BN	1×2208	1×1024
Classifier	output layer	1×1024	$1 \times U$

Table 2: The applied custom Densenet-161-based architecture

(AAMP) (Deng et al., 2019) is adopted as loss function in the training phase of the employed network. It has been in fact shown that such approach guarantees an increase in the Euclidian separation of the produced features, thus reducing intra-class variances while increasing inter-class distances (Deng et al., 2019). The AAMP loss function is therefore recommended to train networks to be employed as feature extractors in biometric systems working in the verification modality, and evaluated according to open-set procedures, in which the subjects exploited for testing purposes and different from those considered during training.

As illustrated in Figure 2, vein features of the enrollment and the query inputs, created by the CNN Feature Embedder, are compared during the testing phase by using Euclidian Distance, after their L_2 normalization[2].

[2]The source code of the employed architectures is available at `https://github.com/ridvansalihkuzu/vein-biometrics`

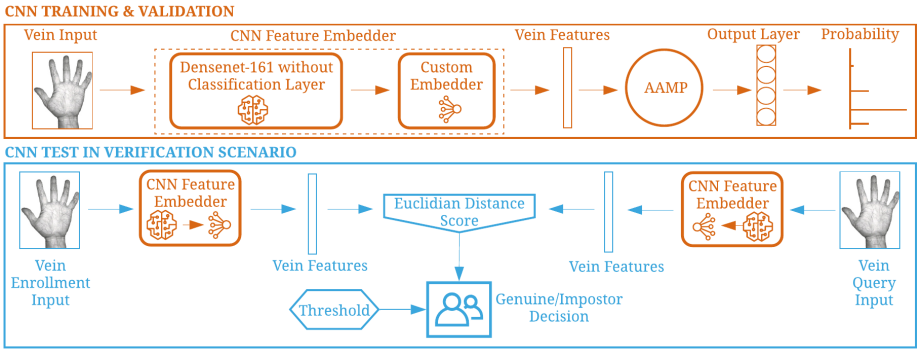

Figure 2: Visual explanation of the training, validation, and testing procedures in the performed tests.

4.2. Network Initialization and Optimization

The adopted CNN is trained for classification purposes, with the features produced by the proposed Custom Embedder taken as generated templates. The loss function adopted for training is the cross-entropy (CE), while back-propagation is performed resorting to stochastic gradient descent (SGD), and using *i)* 32 samples in each batch, *ii)* 0.01 as initial learning rate, reduced tenfold after every 30 epochs, *iii)* a 0.9 momentum, *iv)* 120 training epochs at most, with training stopped in case of minimization of the validation loss.

While searching the best hyper-parameters of AAMP, the penalty margin is selected within the range $m \in [0.3, 0.7]$, while the scale parameter determined within the interval $s \in [16, 96]$.

For the initialization of the Densenet-161 framework, the weights of the Imagenet pre-trained model are used. Moreover, the custom layers defined in the modified Densenet-161 (seen in Table 2) are initialized with *i)* unit weight initialization for BN layers, *ii)* Glorot uniform initialization for FC layers.

5. Experimental analysis and discussion

Our analysis aims at verifying whether vein patterns of one hand of a subject have a greater amount of similarity with the analogous traits of the other hand

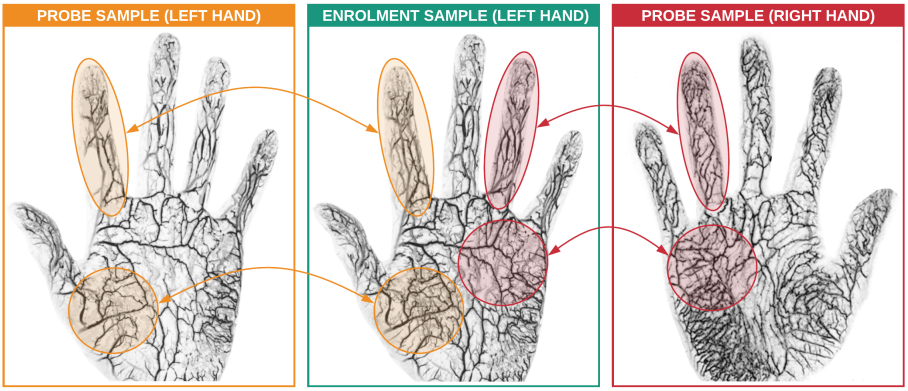

Figure 3: From left to right for one single subject: left hand - first instance, left hand - second instance, right hand.

of the same subject, rather than with the analogous traits of the same hand of a different person. To this aim, several kinds of vein patterns, namely finger, palm, and dorsal hand veins, have been considered in the performed tests. Specifically, as summarized in Table 3, we have estimated different score distributions according to the following scenarios, with some examples graphically depicted in Figure 3:

- *genuine* scores are computed comparing vein patterns extracted from the same finger of the same hand of the same subject. As an example, given a certain subject, comparisons between distinct instances of patterns belonging to the same right index finger are performed. For palm and dorsal vein recognition, genuine scores are computed comparing vein patterns from the same hand of the same individual;
- *impostor* scores are computed, for finger vein recognition, by comparing

Scenario	Subjects	Hands	Fingers	Scores
1	same	same	same	*genuine*
2	different	same	same	*impostor*
3	same	different	same	*genuine CH*
4	different	different	same	*impostor CH*

Table 3: Conditions considered to compute the score distributions.

vein patterns extracted from the same finger of the same hand of different subjects. As an example, veins from the right index of a person are compared against those of a different person's right index. For palm and dorsal vein recognition, impostor scores are computed comparing veins from the same hand of different individuals;

- *genuine cross-hand (CH)* scores are computed, for finger vein recognition and given a certain subject, comparing patterns from corresponding finger from different hands. As an example, veins in the right index are compared against those in the left index of the same person. For palm and dorsal vein recognition, genuine CH scores are computed comparing patterns from different hands of the same subject;

- *impostor CH* scores are computed, for finger vein recognition, by comparing vein patterns extracted from the same finger of different hands of different subjects. As an example, veins in the right index of a person are compared against those of a different person's left index. For palm and dorsal vein recognition, impostor CH scores are computed comparing veins from different hands of different individuals.

The databases employed to estimate the aforementioned score distributions are detailed in Section 5.1. The adopted experimental protocols are then presented in Section 5.2. Vein patterns cross-hand similarity is finally discussed in Section 5.3.

5.1. Employed Databases

In order to provide a comprehensive analysis regarding cross-hand vein pattern similarity, tests have been performed on finger, palm, and dorsal characteristics. To this aim, we have exploited finger vein samples taken from the SDUMLA dataset (Yin et al., 2011), palm vein data from the PolyU-P multispectral dataset (Zhang et al., 2009), dorsal hand vein images from the Bosphorus dataset (Yuksel et al., 2011), and the multi-exposure finger vein dataset captured at Roma Tre University, namely R3VEIN (Kuzu et al., 2020b). For

Benchmark Database	Vein Modality	Database Statistics		Capturing Conditions	Capturing Parts
SDUMLA (Yin et al., 2011)	Finger	# of Subjects	106	grayscale single channel	3 fingers from left and right hands
		# of Classes	636		
		# of Sessions	1		
		Samples per Session	6		
		Total Samples	3.816		
PolyU-P (Zhang et al., 2009)	Palm	# of Subjects	250	4 different spectral channels	left and right hand palms
		# of Classes	500		
		# of Sessions	2		
		Samples per Session	6		
		Total Samples	24.000		
Bosphorus (Yuksel et al., 2011)	Dorsal	# of Subjects	100	4 different environmental conditions	left and right dorsal-hand
		# of Classes	200		
		# of Sessions	1		
		Samples per Session	3		
		Total Samples	1.500		
R3VEIN (Kuzu et al., 2020b)	Finger	# of Subjects	200	4 different channel for varying exposure rates	4-finger images (except thumb) from left and right hand
		# of Classes	400		
		# of Sessions	10		
		Samples per Session	9		
		Total Samples	144.000		

Table 4: Overview of vein databases applied in this study

PolyU-P dataset, only NIR channel images are considered. Similarly, when using the R3VEIN dataset in our experiments, tone-mapped high dynamic range (HDR) samples are generated from 4 images taken at different exposure rates (Kuzu et al., 2020b). The main properties of the considered datasets are summarized in Table 4. All the images of the considered datasets are re-sized into a 224×224 format, and normalized in order to possess zero mean and unitary variance, before using them as input for the considered networks.

5.2. Experimental Framework

Two different CNN training strategies are employed on the considered datasets:

- *Training Strategy-1:* All different hand and fingers are treated as separate classes during training and validation;
- *Training Strategy-2:* different hands of the same user, as well as corresponding fingers from different hands of the same user, are considered as belonging to the same classes during network training and validation. This training strategy is carried out to explicitly trying to extract discriminative features shared by the vein structures in distinct hands of the same individual.

Once the employed network has been trained according to one of the aforementioned strategies, similarity scores belonging to the categories mentioned in Table 3 have been computed over samples considered during the test phases. Once such distributions have been generated, the false rejection rate (FRR) and the false acceptance rate (FAR) associated to the following scenarios have been estimated:

- *Standard comparisons*: as commonly done in biometric recognition testing, each finger or each hand of a subject is considered as a class. FRR and FAR are therefore computed from the *genuine* and *impostor* scores previously defined;

- *Cross-comparisons*: the possibility of interchangeably employing different hands to be recognized, on the basis of the extracted vein patterns, is analyzed by computing the FRR and FAR depending on *genuine CH* and *impostor* scores, or considering *genuine CH* and *impostor CH* scores.

While conducting the experiments, the considered datasets have been divided into two subsets having the same size, and separately uses for training and testing, with 20% of the data selected for training reserved for validation purposes. An open-set scenario has been considered in all the performed tests, taking half of the available classes for training, and leaving the remaining half for testing. When considering databases with multiple sessions, data from distinct sessions have been used for enrollment and verification, with the aim of avoiding any bias effect.

Experiments have been conducted using a dual-processor system equipped with 128Gb RAM, four NVIDIA^{TM} Tesla V100 graphic cards, running under Ubuntu 18.04 LTE OS and using PyTorch 1.4.0.

5.3. Similarity of Cross-Hand Templates

The computed score distributions are shown in Figure 4. Considering the values obtained when employing *Training Strategy-1*, it can be observed that *genuine CH* scores are typically lower than those of *impostor* and *impostor CH*

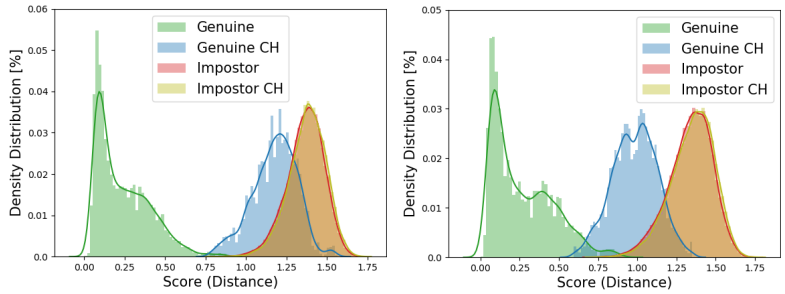

(a) SDUMLA, *Training Strategy-1*

(b) SDUMLA, *Training Strategy-2*

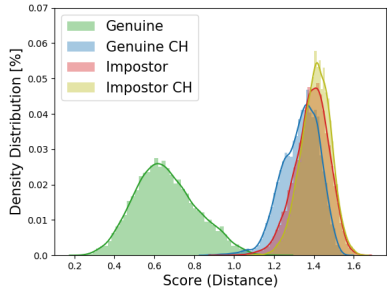

(c) PolyU-P, *Training Strategy-1*

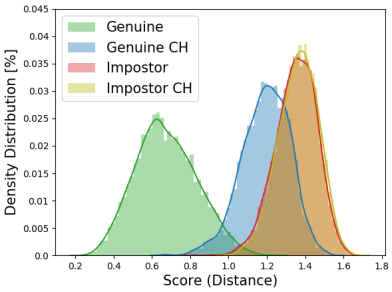

(d) PolyU-P, *Training Strategy-2*

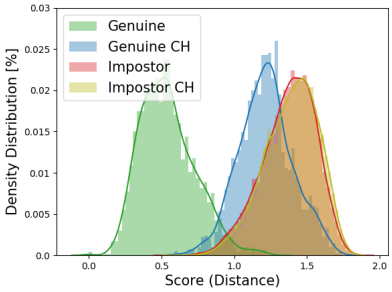

(e) Bosphorus, *Training Strategy-1*

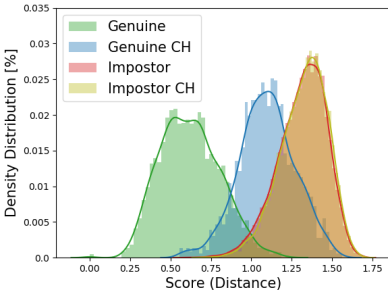

(f) Bosphorus, *Training Strategy-2*

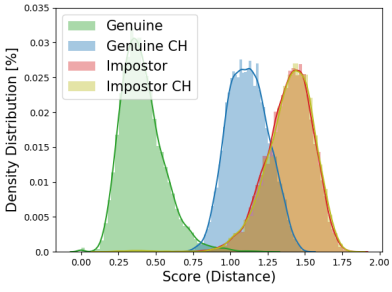

(g) R3VEIN, *Training Strategy-1*

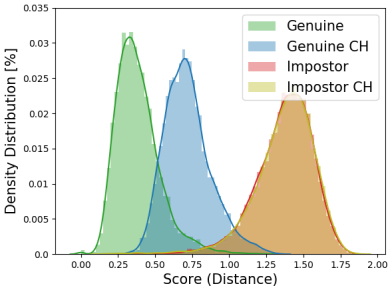

(h) R3VEIN, *Training Strategy-2*

Figure 4: Genuine, Genuine-CH, Impostor, and Impostor CH score distributions for experiments on the considered databases, using *Training Strategy-1* and *Training Strategy-2*.

Databases	Training Strategy-1		Training Strategy-2	
	Standard Comparison	Cross Comparison	Standard Comparison	Cross Comparison
SDUMLA	0.02%	22.1%	0.23%	10.9%
PolyU-P	0.22%	38.5%	0.86%	25.3%
Bosphorus	2.33%	30.8%	2.79%	23.9%
R3VEIN	0.57%	17.6%	1.19%	4.46%

Table 5: EERs (in %) for the performed tests based on different training strategies

distributions. This finding already corroborates the hypothesis that left and right hand vein patterns of the same persons are more similar than those of unrelated persons. This aspect is particularly evident for finger-vein patterns, as shown by the results on SDUMLA and R3VEIN databases.

Furthermore, the scores obtained using *Training Strategy-2* are characterized by a far larger separation between *genuine CH* and *impostor* scores, testifying the effectiveness of the employed training procedure in finding common characteristics in left and right hand vein patterns, while preserving their inter-subject discriminability.

It can also be noticed that *impostor* and *impostor CH* distributions are almost overlapped, for all the considered databases and for both the employed training strategies. Minimal differences can be seen only for PolyU-P and Bosphorus databases, when *Training-Strategy-1* is employed. Using *Training-Strategy-2*, specifically designed to look for similarities in left and right hands, even such slight differences disappear. This behavior means that vein patterns of different persons are so different that it does not matter which hand is used by an attacker for an impostor attempt (given that the system compares mirrored images, in case left and right hands are compared).

The EERs achieved using the recognition strategy detailed in Section 4, for each of the test conditions, are reported in Table 5. The results obtained considering the *Training Strategy-1* scenario show that, when fingers, palm, and dorsal veins from left and right hands are considered as separate classes during training, the recognition performance are quite poor if a palm or a finger is used for enrollment, and the corresponding ones from the other hand are then used for recognition. This can be clearly seen by comparing the recognition

rates achieved in the *standard comparison* and *cross-comparison* test scenarios: considering for instance the SDUMLA dataset, while a low EER at 0.02% is achieved in the former case, a much higher EER at 22.1% is instead obtained when using vein patterns of different hands as genuine samples.

On the other hand, the results obtained exploiting the *Training Strategy-2* scenario show that, when training is performed considering finger, palm, and dorsal veins from left and right hands as belonging to the same class, the recognition performance achieved computing genuine scores from comparisons of vein patterns from different hands is significantly improved, with respect to the previous case. This means that, under *Training Strategy-2*, the employed CNN is actually able to find discriminative characteristics shared between the cross pairs of vein patterns. The receiver operating Characteristic (ROC) curves computed for the considered database, for both the employed training strategies, are depicted in Figure 5.

In more detail, the recognition rates obtained for standard comparisons when considering the *Training Strategy-1* scenario are a bit better than the ones achieved when adopting the *Training Strategy-2*, although these latter are still good for recognition purposes. Nonetheless, the *Training Strategy-2* scenario allows extracting characteristics which could allow to perform a successful matching between vein patters coming from different hands of the same person. It is worth remarking that such possibility can be considered admissible only for finger vein patterns taken from the SDUMLA and R3VEIN dataset, while it is much less practically feasible for vein patterns from the PolyU-P and Bosphorus databases, for which EERs greater than 20% have been achieved when using samples from different hands to compute genuine scores. In more detail, the largest extent of similarities is found when considering samples from the R3VEIN dataset, since the images there collected contain vein patters from four fingers, with therefore much more information with respect to the samples from the SDUMLA dataset. As seen also from the ROC curves in Fig. 5(d), and from the distributions in Fig. 4(h), the scores obtained when performing cross-hand comparisons are quite close to those obtained considering standard

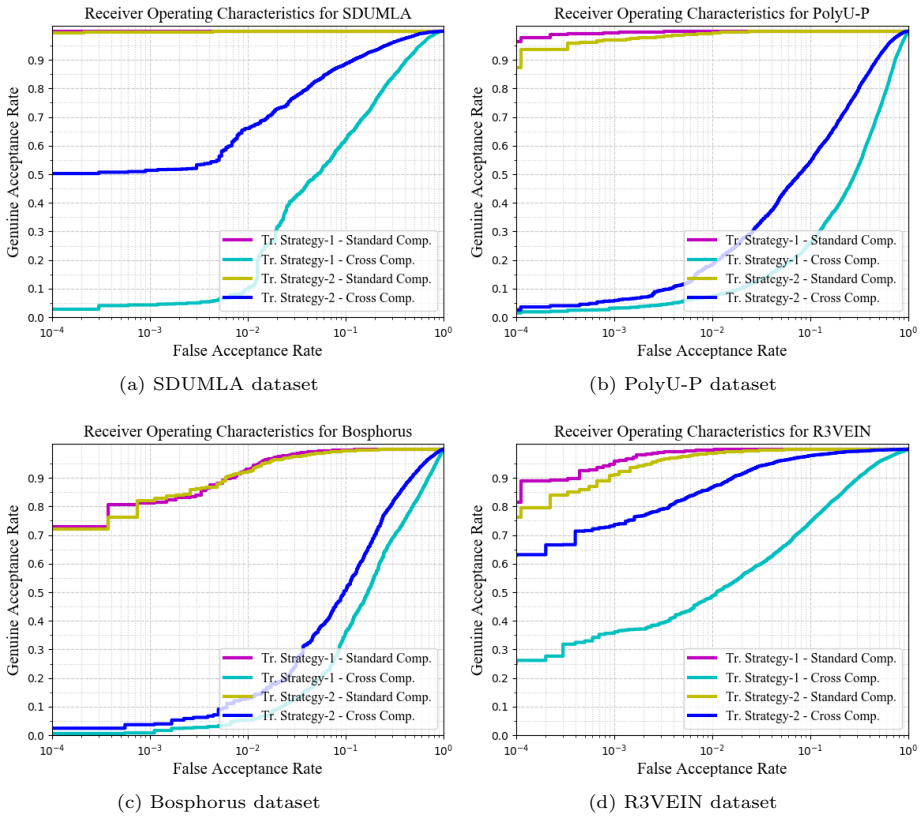

(a) SDUMLA dataset

(b) PolyU-P dataset

(c) Bosphorus dataset

(d) R3VEIN dataset

Figure 5: ROC curves obtained on SDUMLA, PolyU-P, Bosphorus, and R3VEIN datasets, for both the employed training strategies.

genuine comparisons, under *Training Strategy-2*.

A further understanding of the underlying processes can be obtained by checking the activation patterns on vein images obtained when training the employed CNN according to the two adopted training strategies. To this aim, we have computed the gradient-weighted class activation mapping (grad-CAM) (Selvaraju et al., 2017) on the available vein samples, obtaining images such as those shown as examples in Figure 6. In more detail, the upper parts of Figures 6(a) and 6(b) show the results obtained when the vein patterns from different hands are considered as separate classes during training. In this case, the heatmap colour distributions contain more dark-red pixels for both left and right hand samples. This means that the regions including veins give strong

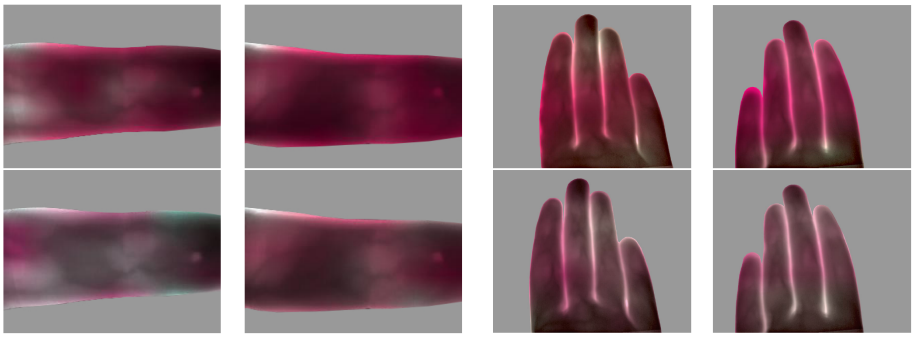

(a) Grad-CAM activation heatmaps on SDUMLA (b) Grad-CAM activation heatmaps on R3VEIN

Figure 6: Grad-CAM activation heatmaps on SDUMLA and R3VEIN database samples: the left and right fingers of the same person are illustrated on the left and right sides of each dataset accordingly; the upper heatmaps for the Training Strategy-1, while the bottom ones for the Training Strategy-2.

contribution to the activation of CNN layers to be distinguished as separate classes. Nevertheless, in case of *Training Strategy-2*, these contributions to the activation of CNN layers fade, as shown in the lower parts of Figure 6(a) and 6(b). This means that taking cross- hand/finger samples as belonging to the same class slightly weakens the separability of classes based on vein patterns.

6. Conclusions

In this study we have investigated, within a biometric recognition framework, the similarity of vein structures across different finger, palm, and dorsal regions. Leveraging on literature studies carrying out similar analysis on several biometric traits, we have resorted to deep learning strategies to better emulate human learning and discriminating capabilities. The results obtained when adopting a standard network training strategy, that is, considering vein patterns from each finger, palm, or dorsum as an independent class, indicate that significant similarities between corresponding vein patterns of different hands exist. Nonetheless, the performance achievable performing recognition using the trait belonging to a hand other than the one employed during enrollment is quite poor.

Conversely, a notable performance improvement has been obtained when the

adopted training strategy uses vein patterns from fingers, palms, and dorsa of left and right hands as belonging to the same class, and genuine scores are computed by comparing vein patterns from different hands. The obtained findings are similar to those given in (Claes et al., 2015) for ear and in (Kumar et al., 2016) for palmprint: in both papers the similarities found in left and right biometric traits allow to compute an EER in the order of 10%, analogous to the one we report for finger-vein data from SDUMLA. An even lower EER has been achieved in our tests over the R3VEIN dataset, which comprises images with four fingers altogether.

A lower amount of similarity has been achieved for palm-vein data from PolyU-P, and for dorsum-vein samples from Bosphorus, with EERs respectively at 25.3% and 23.9%. Therefore, further studies could be beneficial to evaluate whether different approaches would detect higher similarities, while maintaining inter-subject differences, for palm- and dorsal-vein patterns of left and right hands. For instance, the use of deep generative models such as generative adversarial networks (GAN) or autoencoders could be exploited to this aim. These latter could be in fact employed to evaluate whether the vein pattern representation of one hand could be retrieved from the features extracted from the other one, while preserving discriminative capabilities.

Acknowledgements

This work has been partially supported by the H2020 ECSEL EU Project Intelligent Secure Trustable Things (InSecTT). InSecTT (`www.insectt.eu`) has received funding from the ECSEL Joint Undertaking (JU) under grant agreement No 876038. The JU receives support from the European Union's Horizon 2020 research and innovation programme and Austria, Sweden, Spain, Italy, France, Portugal, Ireland, Finland, Slovenia, Poland, Netherlands, Turkey.

The document reflects only the author's view and the Commission is not responsible for any use that may be made of the information it contains.

References

Ahmad, F., Cheng, L.-M., & Khan, A. (2019). Lightweight and Privacy-Preserving Template Generation for Palm-Vein Based Human Recognition. *IEEE Transactions on Information Forensics and Security*, .

Biswas, S., Rohdin, J., Mňuk, T., & Drahanský, M. (2019). Is there any similarity between a person's left and right retina? In *IEEE International Conference of the Biometrics Special Interest Group (BIOSIG)*.

Bowyer, K., Lagree, S., & Fenker, S. (2010). Human versus biometric detection of texture similarity in left and right irises. In *First Int. Workshop on Deep Learning and Pattern Recognition* (pp. 1–7).

Claes, P., Reijniers, J., Shriver, M., Snyders, J., Suetens, P., Nielandt, J., De Tre, G., & Vandermeulen, D. (2015). An investigation of matching symmetry in the human pinnae with possible implications for 3d ear recognition and sound localization. *Journal of Anatomy*, *226*, 60–72.

Das, A., Pal, U., Ballester, M. A. F., & Blumenstein, M. (2014). A New Wrist Vein Biometric System. In *2014 IEEE Symposium on Computational Intelligence in Biometrics and Identity Management (CIBIM)* (pp. 68–75). IEEE.

Daugman, J. (2004). How iris recognition works. *IEEE Transactions on Circuits and Systems for Video Technology*, *14*, 21–30.

Deng, J., Guo, J., Xue, N., & Zafeiriou, S. (2019). Arcface: Additive Angular Margin Loss for Deep Face Recognition. In *Proceedings of the IEEE Conference on Computer Vision and Pattern Recognition* (pp. 4690–4699).

Fang, Y., Wu, Q., & Kang, W. (2018). A Novel Finger Vein Verification System Based on Two-Stream Convolutional Network Learning. *Neurocomputing*, *290*, 100–107.

Hao, Y., Sun, Z., Tan, T., & Ren, C. (2008). Multispectral Palm Image Fusion for Accurate Contact-Free Palmprint Recognition. In *2008 15th IEEE International Conference on Image Processing* (pp. 281–284). IEEE.

Hollingsworth, K., Bowyer, K., Lagree, S., Fenker, S., & Flynn, P. (2011). Genetically identical irises have texture similarity that is not detected by iris biometrics. *Computer Vision and Image Understanding*, *115*, 1493—-1502.

Huang, G., Liu, Z., Van Der Maaten, L., & Weinberger, K. Q. (2017). Densely Connected Convolutional Networks. In *IEEE Conference on Computer Vision and Pattern Recognition*.

International Organization for Standardization (2006). Iso/iec 19795 standard - -information technology–biometric performance testing and reporting – part 1: Principles and framework. *ISO/IEC*, .

Jalilian, E., & Uhl, A. (2018). Finger-Vein Recognition Using Deep Fully Convolutional Neural Semantic Segmentation Networks: The Impact of Training Data. In *2018 IEEE International Workshop on Information Forensics and Security (WIFS)* (pp. 1–8). IEEE.

Kabaciński, R., & Kowalski, M. (2011). Human Vein Pattern Correlation - A Comparison of Segmentation Methods. In *Computer Recognition Systems 4* (pp. 51–59). Springer.

Kauba, C., Piciucco, E., Maiorana, E., Campisi, P., & Uhl, A. (2016). Advanced Variants of Feature Level Fusion for Finger Vein Recognition. In *IEEE International Conference of the Biometrics Special Interest Group (BIOSIG)*.

Kumar, A., Wang, K. et al. (2016). Identifying Humans by Matching their Left Palmprint with Right Palmprint Images using Convolutional Neural Network. In *First International Workshop on Deep Learning and Pattern Recognition*.

Kumar, A., & Zhou, Y. (2011). Human Identification Using Finger Images. *IEEE Transactions on Image Processing*, *21*, 2228–2244.

Kuzu, R. S., Maiorana, E., & Campisi, P. (2020a). Loss Functions for CNN-based Biometric Vein Recognition. In *28th European Signal Processing Conference (EUSIPCO 2020)*.

Kuzu, R. S., Piciucco, E., Maiorana, E., & Campisi, P. (2020b). On-the-fly Finger-Vein-based Biometric Recognition using Deep Neural Networks. *IEEE Transactions on Information Forensics and Security*, *15*, 2641–2654.

Lu, Y., Xie, S. J., Yoon, S., Wang, Z., & Park, D. S. (2013). An Available Database for the Research of Finger Vein Recognition. In *2013 6th International congress on image and signal processing (CISP)* (pp. 410–415). IEEE volume 1.

Miura, N., Nagasaka, A., & Miyatake, T. (2007). Extraction of Finger-Vein Patterns Using Maximum Curvature Points in Image Profiles. *IEICE Transactions on Information and Systems*, *E90-D*, 1185–1194.

Pan, Z., Wang, J., Shen, Z., Chen, X., & Li, M. (2019). Multi-Layer Convolutional Features Concatenation with Semantic Feature Selector for Vein Recognition. *IEEE Access*, *7*, 90608–90619.

Piciucco, E., Kuzu, R. S., Maiorana, E., & Campisi, P. (2019). On the Cross-Finger Similarity of Vein Patterns. In *International Conference on Image Analysis and Processing* (pp. 12–20). Springer.

Qin, H., El-Yacoubi, M. A., Lin, J., & Liu, B. (2019). An Iterative Deep Neural Network for Hand-vein Verification. *IEEE Access*, .

Radzi, S., Khalil-Hani, M., & Bakhteri, R. (2016). Finger-Vein Biometric Identification Using Convolutional Neural Network. *Turkish Journal of Electrical Engineering & Computer Sciences*, *24*, 1863–1878.

Rice, J. (1987). Apparatus for the Identification of Individuals. US Patent 4,699,149.

Selvaraju, R. R., Cogswell, M., Das, A., Vedantam, R., Parikh, D., & Batra, D. (2017). Grad-CAM: Visual Explanations from Deep Networks via Gradient-based Localization. In *Proceedings of the IEEE International Conference on Computer Vision* (pp. 618–626).

Song, J. M., Kim, W., & Park, K. R. (2019). Finger-Vein Recognition Based on Deep DenseNet Using Composite Image. *IEEE Access*, .

Thapar, D., Jaswal, G., Nigam, A., & Kanhangad, V. (2019). PVSNet: Palm Vein Authentication Siamese Network Trained using Triplet Loss and Adaptive Hard Mining by Learning Enforced Domain Specific Features. In *2019 IEEE 5th International Conference on Identity, Security, and Behavior Analysis (ISBA)* (pp. 1–8). IEEE.

Ton, B. T., & Veldhuis, R. N. J. (2013). A High Quality Finger Vascular Pattern Dataset Collected Using a Custom Designed Capturing Device. In *International Conference on Biometrics (ICB)* (pp. 1–5).

Uhl, A., Busch, C., Marcel, S., & Veldhuis, R. (2020). *Handbook of Vascular Biometrics*. Springer Nature.

Wang, G., Sun, C., & Sowmya, A. (2020). Multi-weighted Co-occurrence Descriptor Encoding for Vein Recognition. *IEEE Transactions on Information Forensics and Security*, *15*, 375–390. doi:10.1109/TIFS.2019.2922331.

Wang, J., Pan, Z., Wang, G., Li, M., & Li, Y. (2018). Spatial Pyramid Pooling of Selective Convolutional Features for Vein Recognition. *IEEE Access*, *6*, 28563–28572.

Wang, L., Leedham, G., & Cho, D. S.-Y. (2008). Minutiae Feature Analysis for Infrared Hand Vein Pattern Biometrics. *Pattern Recognition*, *41*, 920–929.

Wu, W., Elliott, S. J., Lin, S., & Yuan, W. (2019). Low-cost Biometric Recognition System based on NIR Palm Vein Image. *IET Biometrics*, *8*, 206–214. doi:10.1049/iet-bmt.2018.5027.

Xie, C., & Kumar, A. (2017). Finger Vein Identification using Convolutional Neural Network and Supervised Discrete Hashing. In *Deep Learning for Biometrics* (pp. 109–132). Springer.

Xu, Y., Fei, L., & Zhang, D. (2015). Combining left and right palmprint images for more accurate personal identification. *IEEE Transactions on on Image Processing*, *24*, 549–559.

Yang, L., Yang, G., Yin, Y., & Xi, X. (2018). Finger Vein Recognition with Anatomy Structure Analysis. *IEEE Transactions on Circuits and Systems for Video Technology*, *28*, 1892–1905.

Yang, W., Hui, C., Chen, Z., Xue, J.-H., & Liao, Q. (2019). FV-GAN: Finger Vein Representation Using Generative Adversarial Networks. *IEEE Transactions on Information Forensics and Security*, .

Yang, W., Yu, X., & Liao, Q. (2009). Personal authentication using finger vein pattern and finger-dorsa texture fusion. In *Proceedings of the 17th ACM international conference on Multimedia* (pp. 905–908).

Yin, Y., Liu, L., & Sun, X. (2011). SDUMLA-HMT: A Multimodal Biometric Database. In *Chinese Conference on Biometric Recognition*.

Yuksel, A., Akarun, L., & Sankur, B. (2011). Hand vein biometry based on geometry and appearance methods. *IET computer vision*, *5*, 398–406.

Zhang, D., Guo, Z., Lu, G., Zhang, L., & Zuo, W. (2009). An Online System of Multispectral Palmprint Verification. *IEEE Transactions on Instrumentation and Measurement*, *59*, 480–490.

Zhong, D., Shao, H., & Du, X. (2019). A Hand-based Multi-biometrics via Deep Hashing Network and Biometric Graph Matching. *IEEE Transactions on Information Forensics and Security*, *14*, 3140–3150.

Zhou, Y., & Kumar, A. (2011). Human Identification Using Palm-Vein Images. *IEEE Transactions on Information Forensics and Security*, *6*, 1259–1274.